Stochastic Optimal Control of a Heave Point Wave Energy Converter Based on a Modified LQG Approach

Sun, Tao; Nielsen, Søren R. K.

Stochastic optimal control of a heave point wave energy converter based on a modified LQG approach

Tao Sun*, Søren R.K. Nielsen

Department of Civil Engineering, Aalborg University, 9000 Aalborg, Denmark

Abstract

The optimal control constrain problem of a wave energy point absorber is constrained due to limited stroke and saturation of the control force actuator. The basic idea of this paper is to control the motion of the absorber by a modified LQG control where the constraints on the displacement and actuator force are approximately considered by counteracting the absorbed power in the objective quadratic functional. Based on rational approximations to the radiation force and the wave load, the integrated dynamic system can be reformulated as a linear stochastic differential equation which is driven by a unit intensity Gaussian white noise. The optimal LQG control force becomes a linear function of the state vector of the integrated system, which can only be partially observed. In order to remedy this problem, the control is combined with a Kalman filter observer. The obtained sub-optimal solution has been compared to the numerical optimal solution obtained by nonlinear programming. With suitable calculated gain parameters, the LQG controller can provide approximately the amount of the averaged absorbed power as that of the numerical optimum.

Keywords: wave energy, heave absorber, modified LQG control, displacement and control force restriction, Kalman filtration

2017 MSC: 00-01, 99-00

---

*Corresponding author.
    Email addresses: `tsu@civil.aau.dk` (Tao Sun), `srkn@civil.aau.dk` (Søren R.K. Nielsen)

1. Introduction

A wave energy converter (WEC) extracts the mechanical energy in the wave motion and converts it into electric energy. Different kinds of WEC devices have been developed such as the oscillating water column plant (Ozkop et al., 2017), overtopping types like the Wave Dragon (Wavedragon, 2005), the Pelamis (Pelamis Wave, 2012), Archimedes Wave Swing (Archimedes Wave Swing, 2004), and the Wave Star Energy plant (Wave Star Energy, 2003).

A wave energy point absorber is a wave energy converter (WEC) with horizontal dimensions significantly smaller than the dominating wave length, which is capable of absorbing energy from waves propagating in arbitrary directions. Especially, a heave absorber is constrained by a mooring system or otherwise to move merely in the vertical direction.

Significant increase of the power take-off (PTO) of a heave absorber may be achieved by using an active vibration control of the vertical motion (Ringwood et al., 2014). In this connection many control strategies typical of the proportional derivative (PD) type have been suggested in the literatures. Nielsen et al. (2013) derived the optimal control law in irregular sea-states for a heave point absorber with non-linear buoyancy in case of no constraints on the displacements and the control force. The optimal control force turns out to make the absorber maximal flexible by eliminating the inertial load and the buoyancy stiffness totally. Further, the control law has feed-back from the present displacement and acceleration of the absorber and a non-causal feedback from the future velocities. Hence, for practical applications the indicated control law requires a prediction of future velocities. The predictor introduces uncertainty in the problem and makes the control sub-optimal.

Generally, there are constraints on the motion of the absorber due to the limited stroke of the actuator of the control system. Similarly, the available control force will be constrained between certain limits due to saturation. Based on the optimal control for the unconstrained case, Sichani et al. (2014) proposed an extension to the unconstrained case, where the displacement were achieved

2

by adding the nonlinear artificial springs to the buoyancy, which were achieved close to the boundaries. Using predictive PD control, Wang et al. (2015) analyzed the motions of a point absorber. Based on truncated Fourier series of the control force and the velocity, the problem is converted to a optimization problem with a convex quadratic objective functional and nonlinear constraints. Cretel et al. (2011) proposed a control scheme to maximize the absorbed energy by a wave energy point absorber based on model predictive control. As a result of the introduction of triangle-hold discretisation approach where the control force and the wave load need to be continuous piecewise linear, the objective functional is reformulated as a convex quadratic function of the increment of the control force. Constraints on the displacement of the absorber and the control force can be enforced to the system by affine inequality constraints on the input increment control force. However, the control law may give rise to feasibility issues for the hard constraints on the control force and may cause large amounts of energy flowing in and out of the system. Especially, it turns out that the instantaneous absorbed power may undergo large negative excursions which is not the care for the optimal control. Li et al. (2012) analyzed the nearly optimal control of wave energy converter with the state and control input constraints based on Pontryagins Minimum Principle. Further, the interior penalty term included in the cost functional replace the state constraints, preventing the optimal state trajectory from approaching the boundary of the permitted region. The nearly optimal control approximated using discretization and dynamic programming turns out to be bang-bang control on the condition that the portions of the singular arc assuming that the times in which this happens are negligible are ignored, without rigorous proof for that. Zou et al. (2017) demonstrated that the singular arc part of the optimal control cannot be neglected and significant portions of time may become on singular arcs depending on the initial conditions and on the maximum control level. Hartl et al. (1995) presented the Pontryagins maximum principle for optimal control problems with both pure state and mixed variables inequality constraints. Further, the mixed constraints are the constraints on control variables that may depend on the state variables

3

and the time.

As the optimal control turns out to be noncausal, i.e. the control law depends on the future motion of the absorber or wave load, prediction of the motion of the absorber or wave load should be considered. To remedy this question, a causal closed-loop controller with the feedback information is proposed. In case of infinite control horizon this problem can be circumvented by LQG control. Lattanzio and Scruggs (2011) derived the optimal causal controller for wave energy converter and the determination of the optimal causal controller distills to a nonstandard LQG optimal control problem, which can be solved easily. Scruggs et al. (2013)formulated the LQG control problem for wave energy converter and compared the results with the optimal noncausal control through choosing proper weights. Kassem et al. (2015) maximized the take-off power from a two-body point absorber with a mooring wave energy converter based on LQG approach and demonstrated the feasibility and effectiveness of the LQG control. In the present paper the basic idea is to deal with stochastic optimal control of a heave point wave absorber with constraints on the displacement and the control force, and with noisy observation on the displacement and the velocity. The radiation force and the wave load are reformulated as output of rational approximate filters. The integrated dynamic system may be given by a linear stochastic state vector differential equation driven by a Gaussian white noise. The idea of the paper is to take the constraints on the displacement and the control force into consideration by introducing negative penalty terms of the two parameters in the Lagrangian of a LQG approach, where the weights are calibrated against a nonlinear programming solution to provide the same mean power take-off. This does not guarantee a local observation of the indicated constraints, but merely that these are fulfilled in average. Further, the controller is combined with a Kalman filter, for which the reason is merely that the displacement and the velocity can be observed. The obtained sub-optimal results from assumed full state observation and partial state observation will be discussed and compared to numerical optimal controller from nonlinear programming. From the performance integral of the optimization problem it is

4

shown in the paper that the displacement constraints cannot be active during a finite time interval. The stochasticity of the control problem origins partially from the nonobservable wave load and the noise related to the measured displacements and velocities. Hence, the indicated quantities need to be modelled by stochastic process.

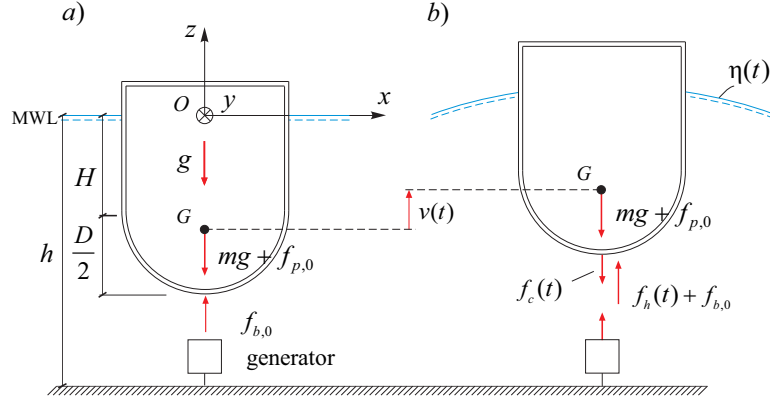## 2. Equation of motion of point absorber

Figure 1: Loads on heave absorber. a) Static equilibrium state. b) Dynamic state.

Although, only the heave absorber shown in Fig. 1 will be analyzed, all results, including the equation of motion and control laws, may easily be carried over to other single-degree-of-freedom systems by slight modifications. The (x, y, z)-coordinate system is introduced as shown in Fig. 1. The original O is placed in the mean water level (MWL) at the centerline of the point absorber. The x-axis is the horizonal orientation in the direction of the wave propagation, and the z-axis is vertical orientation in the upward direction. Only two-dimensional (plane) regular or irregular waves are considered. The motion $v(t)$ of the body in the vertical z direction is defined relative to the static equilibrium state, where the static buoyancy force balances the gravity force and a possible static pre-stressing force from the generator.

5

In the dynamic state caused by the surface elevation $\eta(t)$ the WEC is excited by dynamic hydrodynamic force, $f_h(t)$, in addition to the static buoyancy force, and by an additional control force, $f_c(t)$ from an external hydraulic or electric force generator as the PTO system, which is used to control the motion of the absorber and to achieve maximal wave energy absorption. In theoretical research, it's assumed that the PTO system can provide the reactive power. In applications, the cylinder can operate as a pump, producing a bi-directional flow, which drives a hydraulic motor. The motor adapts to the flow and rectifies the flow into a unidirectional turning of the generator. Further, The PTO system will absorb a positive power from the absorber if the control force $f_c(t)$ and the velocity $\dot{v}(t)$ are in counter phase. In opposite case, the PTO system acts as a motor and supplies energy to the absorber. Next, the mechanical energy stored in the absorber is converted into electrical energy via an generator. Henceforth, $f_c(t)$ considered positive in the opposite direction of $v(t)$ will be referred to as the control force. Then, the equation of motion becomes:

$$m\ddot{v}(t) = f_h(t) - f_c(t) \tag{1}$$

Assuming linear wave theory $f_h(t)$ may be written as a superposition of the following contributions:

$$f_h(t) = f_b(t) + f_r(t) + f_e(t) \tag{2}$$

where $f_b(t)$ is the quasi-static increment of the buoyancy force, $f_r(t)$ is the radiation force generated by the motion of the absorber in still water, and $f_e(t)$ is the wave excitation force caused by the wave action, when the absorber is fixed in the static equilibrium state. The term $f_r(t)$ removes mechanical energy by generating a wave train propagating away from the absorber, whereas $f_e(t)$ supplies energy to the absorber. $f_b(t)$ is given as:

$$f_b(t) = \rho\Big(D\big(v(t)\big) - D(0)\Big)g = -r\big(v(t)\big) \tag{3}$$

where ρ is the mass density of water, and $D\big(v(t)\big)$ denotes the displaced water volume at the displacement $v(t)$. The nonlinear buoyancy function $r\big(v(t)\big)$ is

limited between the value r_1 corresponding to a fully submerged absorber, and the value $r_0 = -f_{b,0}$, when the absorber is jumping out of the water. Assuming small vertical vibrations, Eq. (3) may be linearized around the static equilibrium state as (Newman, 1977):

$$f_b(t) = -k\, v(t) \quad , \quad k = r'(0) = \rho\, D'(0)\, g = \frac{1}{4}\pi D^2 \rho g \tag{4}$$

The radiation force $f_r(t)$ may be written in terms of the following differential-integro relation (Cummins, 1962; Faltinsen, 1990):

$$f_r(t) = -m_h \ddot{v}(t) - f_{r,0}(t) \tag{5}$$

$$f_{r,0}(t) = \int_{-\infty}^{t} h_{r\dot{v}}(t - \tau)\dot{v}(\tau)\, d\tau \tag{6}$$

110   The term m_h is the added water mass at infinite high frequencies, and $h_{r\dot{v}}(t)$ is a causal impulse response function for the radiation force brought forward by the absorber velocity $\dot{v}(\tau)$.

Insertion of Eqs. (3), (5) and (6) in Eq. (1) provides the following integro-differential equation for $v(t)$ driven by $f_e(t)$ and $f_c(t)$:

$$\left. \begin{aligned} \left(m + m_h\right)\ddot{v}(t) + r\big(v(t)\big) + \int_{t_0}^{t} h_{r\dot{v}}(t - \tau)\dot{v}(\tau)\, d\tau = f_e(t) - f_c(t) \ , \ t > t_0 \\ v(t_0) = v_0 , \quad \dot{v}(t_0) = \dot{v}_0 \end{aligned} \right\} \tag{7}$$

where v_0 and $\dot{v}_0$ are given initial conditions at the time t_0.

Due to the causality of the impulse response function, the related frequency response function becomes:

$$H_{r\dot{v}}(\omega) = \int_{0}^{\infty} \mathrm{e}^{-i\omega t} h_{r\dot{v}}(t)\, dt \tag{8}$$

$M_h(\omega)$ and $C_h(\omega)$ denote the hydrodynamic added mass and the hydrodynamic radiation damping coefficient during monochromatic wave excitation. These are related to the imaginary and real parts of $H_{r\dot{v}}(\omega)$ by the following

7

sine and cosine transforms (Nielsen et al., 2013):

$$\left.\begin{array}{l} M_h(\omega) = m_h + \dfrac{1}{\omega}\mathrm{Im}\big(H_{r\dot{v}}(\omega)\big) = m_h - \dfrac{1}{\omega}\displaystyle\int_0^\infty \sin(\omega t)h_{r\dot{v}}(t)\,dt \\[4mm] C_h(\omega) \ = \mathrm{Re}\big(H_{r\dot{v}}(\omega)\big) = \displaystyle\int_0^\infty \cos(\omega t)h_{r\dot{v}}(t)\,dt \end{array}\right\} \tag{9}$$

The wave excitation force $f_e(t)$ may be expressed in terms of the following convolution integral of the sea-surface elevation $\eta(t)$ (Falnes, 2002):

$$f_e(t) = \int_{-\infty}^\infty h_{e\eta}(t-\tau)\eta(\tau)d\tau \tag{10}$$

the sea-surface elevation $\eta(t)$ is assumed to be observed at a sufficient distant position where the measurement is not disturbed by the radiation wave, and $h_{e\eta}(t)$ is a non-causal impulse response function. The related frequency response function becomes:

$$H_{e\eta}(\omega) = \int_{-\infty}^\infty \mathrm{e}^{-i\omega t}h_{e\eta}(t)dt \tag{11}$$

For the indicated heave absorber located in the sea with water depth $h = $
115   30 m, it consists of a cylindrical volume with a diameter $D = 14$ m and a hemisphere with the same diameter as the cylinder. The structural mass m of the absorber is 1.84×10^6kg. The relative physical parameters of the considered point absorber have been defined in the numerical example at the end of the paper. Based on these parameters, the hydrodynamic parameters, i.e. k, m_h,
120   $H_{r\dot{v}}(\omega)$, $H_{e\eta}(\omega)$ can be calculated numerically. In the present case, the program WAMIT has been used, which is based on the boundary element method (WAMIT, 2011). Further, the impulse response functions, $h_{r\dot{v}}(t)$ and $h_{e\eta}(t)$, are obtained by inverse Fourier transform of Eqs. (8) and (11) respectively.

Fig. 2 shows the obtained impulse response function $h_{r\dot{v}}(t)$. The time has
125   been normalized with respect to the peak period T_p. Fig. 3 shows the hydrodynamic added mass. $M_h(\omega) = M_h(-\omega)$ is a an even function of ω, cf. Eq. (9), for which reason only results for positive angular frequencies have been shown. As seen, the asymptotic value m_h is achieved for $\omega \geq 3\omega_p$. Fig. 4 shows the real and imaginary parts of the frequency response function $H_{r\dot{v}}(\omega)$. The real part
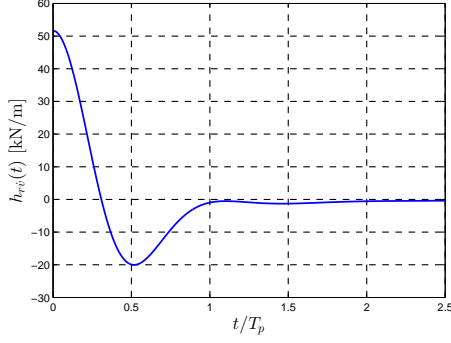130   is a symmetric function and the imaginary part is a show-symmetric function

8

Figure 2: Impulse response function for the radiation force, $h_{r\dot{v}}(t)$.

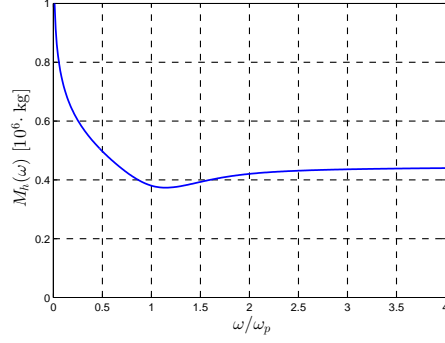

Figure 3: Hydrodynamic added mass, $M_h(\omega)$.

of ω, for which reason only results for positive angular frequencies have been shown. The impulse response function $h_{e\eta}(t)$ for the wave excitation is shown in
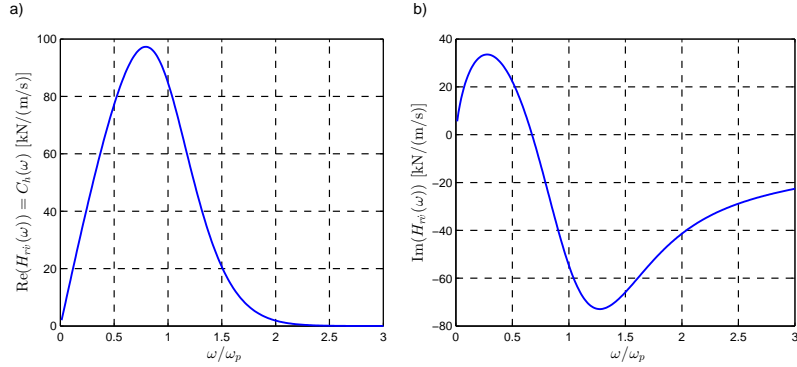

Figure 4: Frequency response function for the radiation force. a) $\text{Re}(H_{r\dot{v}}(\omega))$. b) $\text{Im}(H_{r\dot{v}}(\omega))$.

Fig. 5. The real and imaginary parts of the related frequency response function which will be used in later section for modeling the waves are shown in Figs. 6a) and 6b).

For practical reasons the displacement $v(t)$ will be limited to a finite interval $[v_{\min}, v_{\max}]$, either in order to prevent the absorber form hitting the bottom of the sea or jumping out of the water, or because the actuator has a finite stroke. Similarly, the control force $f_c(t)$ will be constrained to a finite interval
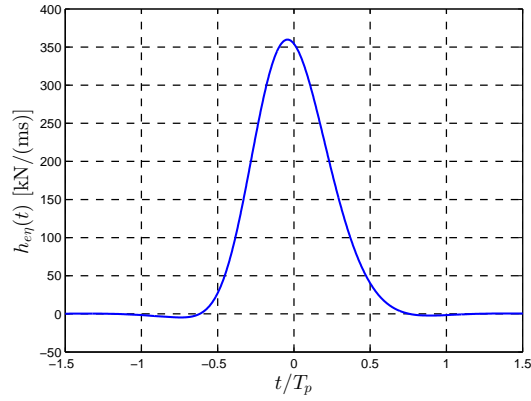
9

Figure 5: Impulse response function for the wave excitation force, $h_{e\eta}(t)$.
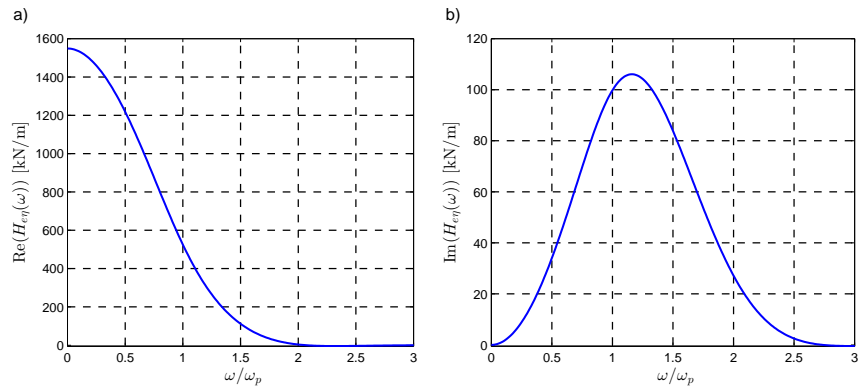

Figure 6: Frequency response function for the wave excitation force. a) $\mathrm{Re}(H_{e\eta}(\omega))$. b) $\mathrm{Im}(H_{e\eta}(\omega))$.

10

$[f_{c,\min}, f_{c,\max}]$ due to saturation in the hydraulic actuator system. Then, based on Eq. (7), the optimal control force which maximizes the absorbed energy during the control interval $[t_0, t_1]$ is obtained as the solution to the following constrained optimization problem:

$$\max \quad J[f_c(t), \dot{v}(t)] = \int_{t_0}^{t_1} f_c(\tau)\dot{v}(\tau)\,d\tau$$

s.t.

$$\begin{cases} (m + m_h)\ddot{v}(t) + r(v(t)) + \int_{t_0}^{t} h_{r\dot{v}}(t - \tau)\dot{v}(\tau)\,d\tau = f_e(t) - f_c(t) \\ v(t_0) = v_0 \ , \dot{v}(t_0) = \dot{v}_0 \\ v_{\min} \leq v(t) \leq v_{\max} \\ f_{c,\min} \leq f_c(t) \leq f_{c,\max} \end{cases} \tag{12}$$

Below, merely an infinite control horizon is considered corresponding to $t_0 = -\infty$ and $t_1 = \infty$. Further, a linear buoyancy restoring force is assumed as indicated in Eq. (4).

3. Rational approximations to the radiation force and the external wave load

For the application in time-domain simulation, control and optimization problem, the integral part of the radiation force, i.e. $f_{r,0}(t)$ in Eq. (6) is replaced by an equivalent system of coupled first-order differential equations. This is equivalent to replacing the frequency response function $H_{r\dot{v}}(\omega)$ by an approximating rational function:

$$H_{r\dot{v}}(\omega) \simeq \tilde{H}_{r\dot{v}}(\omega) = \frac{P(z)}{Q(z)} \quad , \quad z = i\omega \tag{13}$$

$$\left. \begin{array}{l} P(z) = p_0 z^m + p_1 z^{m-1} + \cdots + p_{m-1}z + p_m \\ Q(z) = z^n + q_1 z^{n-1} + \cdots + q_{n-1}z + q_n \end{array} \right\} \tag{14}$$

11

where the parameters $p_0, p_1, \cdots, p_m$ and $q_1, q_2, \cdots, q_n$ are all real. The denominator polynomial may be given on the form:

$$Q(z) = (z - z_1)(z - z_2) \cdots (z - z_n) \tag{15}$$

In order to ensure the stability and strict causality, the order of the filter given by the pair (m, n) should satisfy the condition that $m < n$ and the poles of the denominator z_j must fulfill $\mathrm{Re}(z_j) < 0$. The solution can be obtained by the MATLAB control toolbox (Mathworks, 2011). In Fig. 7 the obtained rational approximation of the order $(m, n) = (2, 3)$ to $H_{r\dot{v}}(\omega)$ is compared with the target frequency response function.
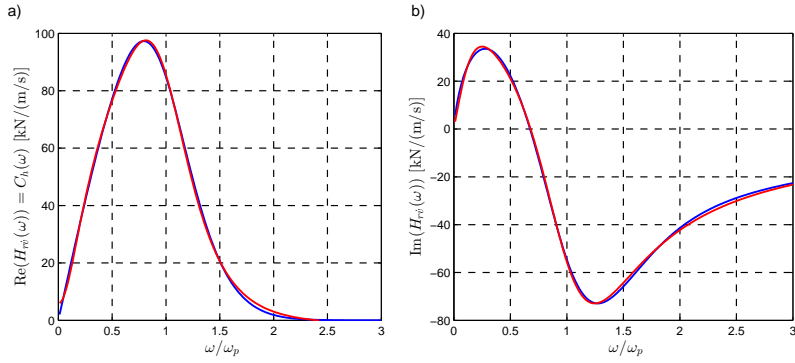

Figure 7: The accuracy of the rational approximation to $H_{r\dot{v}}(\omega)$. a) $\mathrm{Re}(H_{r\dot{v}}(\omega))$. b) $\mathrm{Im}(H_{r\dot{v}}(\omega))$. ———: Numerical determined target frequency function. ———: Rational approximation, $(m, n) = (2, 3)$.

Then, the relation between $f_{r,0}(t)$ and $\dot{v}(t)$ can be expressed by the differential equations:

$$\left. \begin{aligned} f_{r,0}(t) &= p_0 \frac{d^m y(t)}{dt^m} + p_1 \frac{d^{m-1} y(t)}{dt^{m-1}} + \cdots + p_{m-1} \frac{dy(t)}{dt} + p_m y(t) \\ \frac{d^n y(t)}{dt^n} &+ q_1 \frac{d^{n-1} y(t)}{dt^{n-1}} + \cdots + q_{n-1} \frac{dy(t)}{dt} + q_n y(t) = \dot{v}(t) \end{aligned} \right\} \tag{16}$$

where $y(t)$ is an auxiliary function. A harmonic varying input $\dot{v}(t) = \mathrm{Re}(\dot{V} e^{i\omega t})$ to the 2nd equation produces a harmonic varying force $f_{r,0}(t) = \mathrm{Re}(F_{r,0} \, e^{i\omega t})$, $F_{r,0} = \tilde{H}_{r\dot{v}}(\omega)\dot{V}$, of the 1st equation, where $\tilde{H}_{r\dot{v}}(\omega)$ is given by Eqs. (13) and (14).

Eq. (16) can be written on the following state vector form:

$$\frac{d}{dt}\mathbf{z}_r(t) = \mathbf{A}_r\mathbf{z}_r(t) + \mathbf{b}_r\dot{v}(t) \tag{17}$$

$$f_{r,0}(t) = \mathbf{p}_r\mathbf{z}_r(t) \tag{18}$$

where $\mathbf{z}_r(t)$, $\mathbf{A}_r$, $\mathbf{b}_r$ and $\mathbf{p}_r$ can be found in detail in the reference (Nielsen et al., 2013).

In applications the stochastic wave load $f_e(t)$ can be modelled as a zero-mean, stationary Gaussian stochastic process, obtained as the output process of a unit intensity Gaussian white noise process $w_1(t)$, with the frequency response function $H_{ew_1}(\omega)$, passed through a time-invariant physically realizable rational filter. The mean value and auto-covariance function of $w_1(t)$ is given as (Nielsen and Zhang, 2017):

$$\left.\begin{aligned} E[w_1(t)] &= 0 \\ E[w_1(t_1)w_1(t_2)] &= \delta(t_2 - t_1) \end{aligned}\right\} \tag{19}$$

where $E[\cdot]$ is the expectation operator and $\delta(\cdot)$ indicates the Dirac's delta function.

Furthermore, the auto-spectral density function for wave load can be expressed as (Nielsen and Zhang, 2017):

$$S_{f_e f_e}(\omega) = |H_{e\eta}(\omega)|^2 S_{\eta\eta}(\omega) = |H_{ew_1}(\omega)|^2 S_{w_1 w_1} \tag{20}$$

where $S_{f_e f_e}(\omega)$ is double-sided auto spectral density function of wave excitation, and $S_{w_1 w_1} = \frac{1}{2\pi}$ is the double-sided auto spectral density function of unit intensity Gaussian white noise $w_1(t)$. $H_{e\eta}(\omega)$ and $H_{ew_1}(\omega)$ are impulse response functions for the wave excitation force caused by wave height and white noise, respectively. $S_{\eta\eta}(\omega)$ is the double-sided JONSWAP auto spectral density function given as (Hasselmann et al., 1973):

$$S_{\eta\eta}(\omega) = \alpha \frac{H_s^2}{\omega_p} \gamma^\beta \left(\frac{|\omega|}{\omega_p}\right)^{-5} \exp\left(-\frac{5}{4}\left(\frac{\omega}{\omega_p}\right)^{-4}\right) \tag{21}$$

13

where

$$\left.\begin{aligned} \alpha &= \frac{0.0312}{0.230 + 0.0336\gamma - \frac{0.185}{1.9+\gamma}} \\ \beta &= \exp\left(-\frac{1}{2}\left(\frac{|\omega| - \omega_p}{\sigma\omega_p}\right)^2\right) \\ \sigma &= \begin{cases} 0.07 &, \quad |\omega| \le \omega_p \\ 0.09 &, \quad |\omega| > \omega_p \end{cases} \end{aligned}\right\} \tag{22}$$

T_p is the peak period, $\omega_p = \frac{2\pi}{T_p}$ is the related angular peak frequency and H_s is the significant wave height. γ is the so-called peak enhancement parameter which controls the bandwidth of the spectrum. Small and large values of γ represents broad-and narrow-bandedness of the surface elevation spectrum.

Fig. 8 shows the one-sided auto spectral density function of the surface elevation process $S_\eta(\omega)$ and the wave excitation process $S_{f_e}(\omega)$. Both spectrums have been normalized with respect to the angular peak frequency ω_p. As seen $S_{f_e}(\omega) \simeq 0$ for $\omega < 0.5\omega_p$ and $\omega > 1.5\omega_p$. In contrast, the surface elevation process is vanishing for $\omega \ge 3.0\omega_p$.
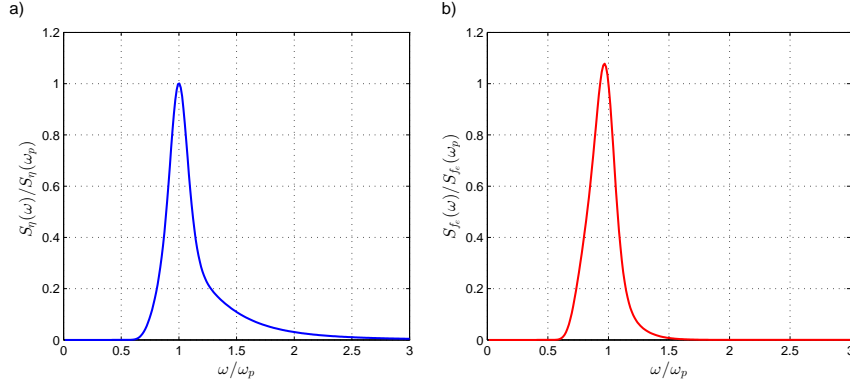
Figure 8: One-sided normalized auto-spectral density functions. a) Surface elevation process. b) Wave excitation process.

In analogy to Eq. (13), the frequency response function $H_{ew_1}(\omega)$ of the filter is approximated by a casual rational function:

$$H_{ew_1}(\omega) = \frac{P(z)}{Q(z)} = \frac{p_0 z^r + p_1 z^{r-1} + \cdots + p_{r-1}z + p_r}{z^s + q_1 z^{s-1} + \cdots + q_{s-1}z + q_s} \quad , \quad z = i\omega \tag{23}$$

14

The filter coefficients are obtained by solving the following optimization problem (Nielsen and Zhang, 2017):

$$\min_{\substack{p_0,\ldots,p_r \\ q_1,\ldots,q_s}} \int_{-\infty}^{\infty} \left(S_{f_e f_e}(\omega) - \frac{1}{2\pi} \frac{P(i\omega)P(-i\omega)}{Q(i\omega)Q(-i\omega)} \right)^2 d\omega \tag{24}$$

s.t.

$$\left. \begin{aligned} \frac{1}{2\pi} \frac{P(i\omega_p)P(-i\omega_p)}{Q(i\omega_p)Q(-i\omega_p)} &= S_{f_e f_e}(\omega_p) \\ \mathrm{Re}(z_j) &< 0, \ j = 1, 2, \cdots, s \end{aligned} \right\} \tag{25}$$

where $z_j, j = 1, 2, \cdots, s$ indicates the poles of the denominator polynomial $Q(z)$, cf. Eq. (15).
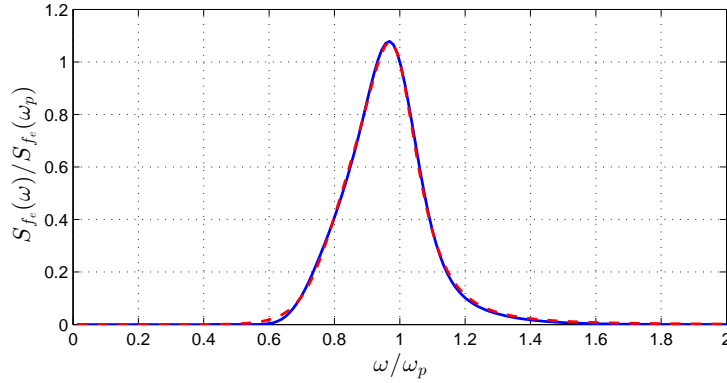
Figure 9: Rational approximation to the one-sided auto-spectral density function of the wave load.

———: Numerical determined target auto-spectral density function. ———: Rational approximation, $(r, s) = (2, 4)$.

The constraint on z_j in Eq. (25) ensures that the filter becomes causal, in contrast to the underlying non-causal filter problem. Nevertheless, the obtained load process will be a zero-mean Gaussian process with the same covariance structure as the original process within the accuracy approximation of the rational auto-spectral density function to the target spectrum. Hence, these processes will be equivalent with probability 1. Fig. 9 illustrates the accuracy of

the rational auto-spectral density function for $(r, s) = (2, 4)$ in comparison to the target auto-spectral density function.

Next, the wave load $f_e(t)$ is obtained from the following state vector equations:

$$\frac{d}{dt}\mathbf{z}_e(t) = \mathbf{A}_e\mathbf{z}_e(t) + \mathbf{b}_e w_1(t) \tag{26}$$

$$\mathbf{z}_e(t) = \begin{bmatrix} y(t) \\ \frac{d}{dt}y(t) \\ \frac{d^2}{dt^2}y(t) \\ \vdots \\ \frac{d^{s-2}}{dt^{n-2}}y(t) \\ \frac{d^{s-1}}{dt^{n-1}}y(t) \end{bmatrix}, \quad \mathbf{b}_e = \begin{bmatrix} 0 \\ 0 \\ 0 \\ \vdots \\ 0 \\ a_1 \end{bmatrix} \tag{27}$$

$$\mathbf{A}_e = \begin{bmatrix} 0 & 1 & 0 & \cdots & 0 & 0 \\ 0 & 0 & 1 & \cdots & 0 & 0 \\ \vdots & \vdots & \vdots & \ddots & \vdots & \vdots \\ 0 & 0 & 0 & \cdots & 0 & 1 \\ -q_s & -q_{n-1} & -q_{s-2} & \cdots & -q_2 & -q_1 \end{bmatrix} \tag{28}$$

$$f_e(t) = \mathbf{p}_e\mathbf{z}_e(t) \tag{29}$$

where:

$$\mathbf{p}_e = \begin{bmatrix} p_r & p_{r-1} & \cdots & p_1 & p_0 & 0 & \cdots & 0 \end{bmatrix} \tag{30}$$

175 a_1 notifies the intensity of the white noise process .

The equation for the integrated dynamic system made up of the displacement $v(t)$ and the velocity $\dot{v}(t)$ of the point absorber, and the state vector $\mathbf{z}_r(t)$ and $\mathbf{z}_e(t)$ of the rational approximations of the radiation force and the wave load may be formulated as:

$$\dot{\mathbf{z}}(t) = \mathbf{A}\mathbf{z}(t) + \mathbf{b}_{f_c}f_c(t) + \mathbf{b}_1 w_1(t) \tag{31}$$

16

where:

$$
\mathbf{z}(t) = \begin{bmatrix} v(t) \\ \dot{v}(t) \\ \mathbf{z}_r(t) \\ \mathbf{z}_e(t) \end{bmatrix}, \mathbf{b}_{f_c} = \begin{bmatrix} 0 \\ -\frac{1}{m_0} \\ \mathbf{0} \\ \mathbf{0} \end{bmatrix}, \mathbf{b}_1 = \begin{bmatrix} 0 \\ 0 \\ \mathbf{0} \\ \mathbf{b}_e \end{bmatrix}, \mathbf{A} = \begin{bmatrix} 0 & 1 & \mathbf{0} & \mathbf{0} \\ -\frac{k}{m_0} & 0 & -\frac{\mathbf{p}_r}{m_0} & \frac{\mathbf{p}_e}{m_0} \\ 0 & \mathbf{b}_r & \mathbf{A}_r & \mathbf{0} \\ \mathbf{0} & \mathbf{0} & \mathbf{0} & \mathbf{A}_e \end{bmatrix}
$$

(32)

where $m_0 = m + m_h$. The dimension of the state vector $\mathbf{z}(t)$ is $N = 2 + n + s$.

4. Modified linear quadratic Gaussian control

In order to obtain the optimal control force, which maximizes the absorbed energy during the control interval $[t_0, t_1]$ and simultaneously reduces the variation of the displacement and control force, the following modified performance functional is applied:

$$
\begin{aligned}
\max \quad J_1[f_c(t), \dot{v}(t), v(t)] &= \frac{1}{2} \int_{-\infty}^{\infty} \big(-qv^2(t) + 2v(t)f_c(t) - rf_c^2(t) \big) dt \\
&= \frac{1}{2} \int_{-\infty}^{\infty} \big(-\mathbf{z}(t)^T \mathbf{Q}\mathbf{z}(t) + 2\mathbf{z}(t)^T \mathbf{p}f_c(t) - rf_c^2(t) \big) dt
\end{aligned}
$$

(33)

where $\mathbf{Q}$ and $\mathbf{p}$ are given as:

$$
\mathbf{Q} = \begin{bmatrix} q & 0 & 0 & \cdots & 0 \\ 0 & 0 & 0 & \cdots & 0 \\ \vdots & \vdots & \vdots & \ddots & \vdots \\ 0 & 0 & 0 & \cdots & 0 \end{bmatrix}, \quad \mathbf{p} = \begin{bmatrix} 0 & 1 & \cdots & 0 \end{bmatrix}^T
$$

(34)

Traditional LQG optimization merely considers the 1st and 3rd terms in the objective functional. In the present case the 2nd term has been introduced to optimize the energy absorbtion, keeping the displacement and the control force as small as possible.

In order to solve the control problem, the variational approach will be adopted. The Hamiltonian of the control problem is defined as:

$$\mathbf{H}(\mathbf{z}(t), f_c(t), \boldsymbol{\lambda}(t), t) = \frac{1}{2}\left(-\mathbf{z}(t)^T \mathbf{Q}\mathbf{z}(t) + 2\mathbf{z}(t)^T \mathbf{p} f_c(t) - r f_c^2(t)\right) \\ + \boldsymbol{\lambda}^T(t)\mathbf{g}(\mathbf{z}(t), f_c(t), t) \tag{35}$$

where $\boldsymbol{\lambda}(t) = [\lambda_v(t), \lambda_{\dot{v}}(t), \boldsymbol{\lambda}_r(t), \boldsymbol{\lambda}_e(t)]^T$ is the co-state vector (Lagrange multiplier). $\mathbf{g}(\mathbf{z}(t), f_c(t), t)$ is given as:

$$\mathbf{g}(\mathbf{z}(t), f_c(t), t) = \mathbf{A}\mathbf{z}(t) + \mathbf{b}_{f_c} f_c(t) + \mathbf{b}_1 w_1(t) \tag{36}$$

The Euler-Lagrange equations for optimal control become (Meirovitch, 1990): Co-state vector equation:

$$\dot{\boldsymbol{\lambda}}(t) = -\frac{\partial H}{\partial \mathbf{z}} \tag{37}$$

Stationarity condition on the control force:

$$\frac{\partial H}{\partial f_c} = 0 \tag{38}$$

Due to the infinite control horizon the transversality condition $\lambda(\infty) = \mathbf{0}$ can be ignored.

Eq. (37) yields the following differential equation for the co-state vector:

$$\dot{\boldsymbol{\lambda}}(t) = -\mathbf{A}^T \boldsymbol{\lambda}(t) + \mathbf{Q}\mathbf{z}(t) - \mathbf{p} f_c(t) \tag{39}$$

Eq. (38) provides the following solution for the optimal control force:

$$f_c(t) = \frac{1}{r}\left(\mathbf{b}_{f_c}^T \boldsymbol{\lambda}(t) + \mathbf{p}^T \mathbf{z}(t)\right) \tag{40}$$

In agreement with the conventional LQG procedure the following solution is assumed for the co-state vector at optimal control:

$$\boldsymbol{\lambda}(t) = -\mathbf{S}(t)\mathbf{z}(t) \tag{41}$$

leading to the following control law:

$$f_c(t) = -\frac{1}{r}\left(\mathbf{b}_{f_c}^T \mathbf{S}(t) - \mathbf{p}^T\right)\mathbf{z}(t) = -\mathbf{G}(t)\mathbf{z}(t) \tag{42}$$

where $\mathbf{G}(t)$ is the control gain matrix given by:

$$\mathbf{G}(t) = \frac{1}{r}\left(\mathbf{b}_{f_c}^T \mathbf{S}(t) - \mathbf{p}^T\right) \tag{43}$$

Substitution of Eqs. (41) and (42) into Eq. (39) provides the following matrix differential equation for $\mathbf{S}(t)$:

$$-\dot{\mathbf{S}}(t)\mathbf{z}(t) - \mathbf{S}(t)\left(\mathbf{A}\mathbf{z}(t) + \mathbf{b}_{f_c}f_c(t) + \mathbf{b}_1 w_1(t)\right) = \mathbf{A}^T \mathbf{S}(t)\mathbf{z}(t) + \mathbf{Q}\mathbf{z}(t) - \mathbf{p}f_c(t) \tag{44}$$

$f_c(t)$ in Eq. (44) is eliminated by Eq. (42). Then, in the stationary state corresponding to infinite control horizon, the matrix $\mathbf{S}$ is obtained from the following Lyapunov equation:

$$\mathbf{S}\mathbf{A} + \mathbf{A}^T \mathbf{S} - \frac{1}{r}\left(\mathbf{S}\mathbf{b}_{f_c} - \mathbf{P}\right)\left(\mathbf{b}_{f_c}^T \mathbf{S} - \mathbf{p}^T\right) + \mathbf{Q} = \mathbf{0} \tag{45}$$

Eq. (45) represents a generalization to the stationary Riccati equation related to standard LQG control. Normally, the information about the future system matrices is required when the Ricatti equation is solved in order to synthesize the optimal control gain at the present time instant (Basu and Staino, 2016). In this paper, assuming the stationary state for the Riccati equation (44), corresponding to infinite control horizon, the control problem becomes causal.

5. State observation based on Kalman filtration

The control law in Eq. (42) represents that the full state state vector $\mathbf{z}(t)$ can be observed. In reality merely the components $v(t)$ and $\dot{v}(t)$ are available. For this reason the control law in Eq. (42) is combined with a Kalman filter state observer. The following observer equation is assumed:

$$\mathbf{y}(t) = \mathbf{C}\mathbf{z}(t) + \mathbf{w}(t) \tag{46}$$

where:

$$\mathbf{y}(t) = \begin{bmatrix} v(t) \\ \dot{v}(t) \end{bmatrix}, \ \mathbf{C} = \begin{bmatrix} 1 & 0 & \mathbf{0} & \mathbf{0} \\ 0 & 1 & \mathbf{0} & \mathbf{0} \end{bmatrix}, \ \mathbf{w}(t) = \begin{bmatrix} a_2 & 0 \\ 0 & a_3 \end{bmatrix}\begin{bmatrix} w_2(t) \\ w_3(t) \end{bmatrix} \tag{47}$$

19

$w_2(t)$ and $w_3(t)$ are mutual independent unit intensity Gaussian white noise processes, cf, Eq. (19). a_2 and a_3 are corresponding intensities indicating the level of the noise.

Let $\mathbf{e}(t)$ be the observer error vector, defined as:

$$\mathbf{e}(t) = \mathbf{z}(t) - \hat{\mathbf{z}}(t) \tag{48}$$

The observer equation becomes (Meirovitch, 1990):

$$\dot{\hat{\mathbf{z}}}(t) = (\mathbf{A} - \mathbf{K}\mathbf{C})\hat{\mathbf{z}}(t) + \mathbf{b}_{f_c} f_c(t) + \mathbf{K}\mathbf{y}(t) \tag{49}$$

where $\hat{\mathbf{z}}(t)$ is the estimated state vector. The estimated control force $\hat{f}_c(t)$ is given as:

$$\hat{f}_c(t) = -\mathbf{G}\hat{\mathbf{z}}(t) \tag{50}$$

and the Kalman gain matrix $\mathbf{K}$ is expressed as:

$$\mathbf{K} = \mathbf{D}\mathbf{C}^T\mathbf{W}^{-1} \tag{51}$$

where $\mathbf{D}$ is the steady-state variance matrix of $\mathbf{e}(t)$ satisfying the Lyapunov equation:

$$\mathbf{A}\mathbf{D} + \mathbf{D}\mathbf{A}^T + \mathbf{V} - \mathbf{D}\mathbf{C}^T\mathbf{W}^{-1}\mathbf{C}\mathbf{D} = \mathbf{0} \tag{52}$$

where $\mathbf{V}$ and $\mathbf{W}$ are the intensities of the process $w_1(t)$ and $\mathbf{w}(t)$, which can be expressed as:

$$\mathbf{V} = a_1^2\mathbf{b}_1\mathbf{b}_1^T, \ \mathbf{W} = \left[\begin{array}{cc} a_2^2 & 0 \\ 0 & a_3^2 \end{array} \right] \tag{53}$$

6. Numerical example

A point heave wave energy converter is considered in the numerical simulation. The relevant data of the absorber and the wave excitation parameters have been indicated in Table 1.

In the following the accuracy of the theory will be tested against numerical results obtained by nonlinear programming. The nonlinear programming formulation of the optimal control problem is related to two approximations related to

20

Table 1: Heave absorber and wave excitation parameters

Parameter	Value	Unit	Parameter	Value	Unit
H	7.00	m	$v_{\max}$	0.50	m
D	14.00	m	$v_{\min}$	-0.50	m
h	30.00	m	$f_{c,\max}$	4.0×10^5	N
m	1.84×10^6	kg	$f_{c,\min}$	-4.0×10^5	N
m_h	0.44×10^6	kg	q	9.00×10^5	N/(ms)
H_s	3.00	m	r	3.00×10^{-7}	m/(Ns)
T_p	7.42	s	a_2	0.50	ms$^{1/2}$
γ	5		a_3	0.50	ms$^{-1/2}$

the state vector representation in Eqs. (17) and (18) of the convolution integral for the radiation force, and to a discretization of the performance functional iat instants of time separated by the interval $\Delta\tau$.

In order to check the accuracy in the nonlinear programming algorithm, it has been checked against the theoretical solution for optimal control of the unconstrained heave absorber due to Nielsen et al. (2013), given as:

$$f_c(t) = -(m + m_h)\ddot{v}(t) - kv(t) + \int_t^\infty h_{r\dot{v}}(\tau - t)\dot{v}(\tau)\,d\tau \qquad (54)$$

Fig. 10 shows the results for a time step $\Delta\tau = \frac{T_p}{150}$ in the discretization of the control interval, and a rational approximation of the order $(m, n) = (2, 3)$ for the convolution integral. The nonlinear programming solution at optimal control for $v(t), \dot{v}(t)$ and $\ddot{v}(t)$ were used at calculation of the theoretical solution.

Figs. 11a and 11b show the displacement and velocity of the absorber under LQG control for full and partial state observation, corresponding to Eqs. (42) and (50), with the indicated parameters, and the comparison with nonlinear programming as formulated in appendix.

Fig. 11c indicates the corresponding control force. Fig. 11d and Table 2 indicate the instantaneous power and mean power based on LQG control. As seen, the partial observation merely reduce the mean absorbed power due to the
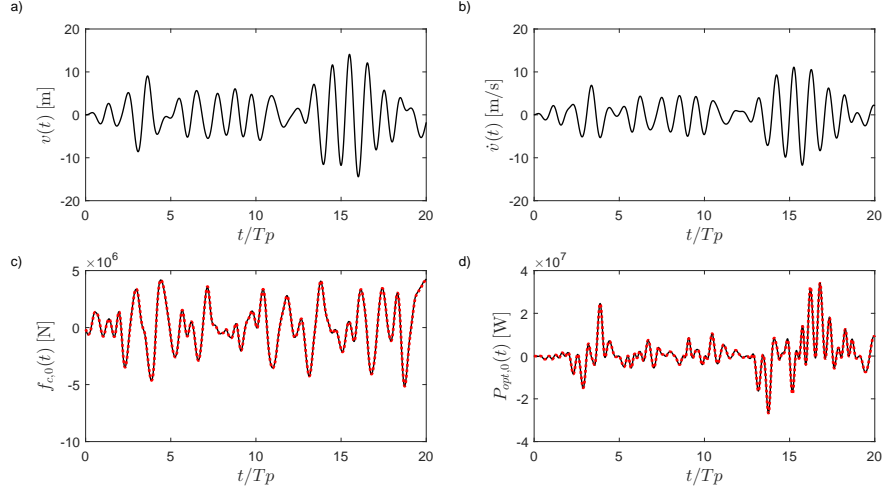
Figure 10: Unconstrained case. The trajectories, control force and instantaneous absorbed power at optimal control. a) $v(t)$. b) $\dot{v}(t)$. c) $f_{c,0}(t)$. d) $P_{\mathrm{opt},0}(t)$. ——: Nonlinear programming solution. ·······: Unconstrained analytical solution (Nielsen et al, 2013).
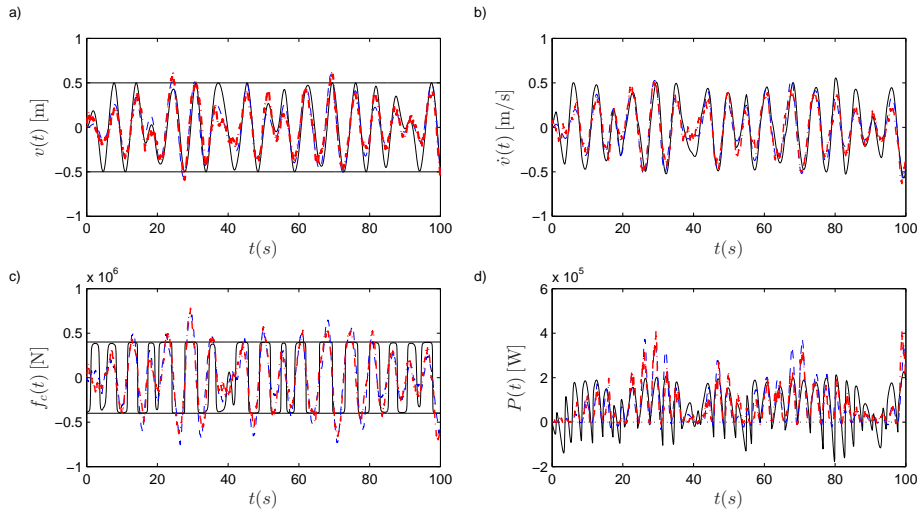

Figure 11: The trajectories of $v(t)$ and $\dot{v}(t)$, control force $f_c(t)$ and instantaneous absorbed power $P(t)$ at optimal control. $H_s = 3$m, $T_p = 7.42$s and $\gamma = 5$. $f_{c,\max} = -f_{c,\min} = 4 \times 10^5$N and $v_{\max} = -v_{\min} = 0.5$m. a) $v(t)$. b) $\dot{v}(t)$. c) $f_c(t)$. d) $P(t)$. ——: Nonlinear programming solution. – – –: LQG, full state observation. –·–·–: LQG, partial state observation.

22

Table 2: Mean absorbed power under different wave conditions

	$\gamma = 5$	$\gamma = 1$
Nonlinear programming	78.1005 kW	84.3520 kW
LQG, full state observation	77.0597 kW	83.3994 kW
LQG, partial state observation with (a_2, a_3)=(0.05ms$^{1/2}$, 0,05ms$^{-1/2}$)	73.4893 kW	80.4685 kW
LQG, partial state observation with (a_2, a_3)=(0.5ms$^{1/2}$, 0,5ms$^{-1/2}$)	61.3112 kW	76.2606 kW

limited state observation. In order to evaluate the effect of a_2 and a_3 on the absorbed power, two pairs (a_2, a_3) are compared.

In Table 2, the absorber power with $(a_2, a_3) = (0.50 \, \text{ms}^{1/2}, 0.50 \, \text{ms}^{-1/2})$ is larger than the absorbed power with $(a_2, a_3) = (1.00 \, \text{ms}^{1/2}, 1.00 \, \text{ms}^{-1/2})$. It can be known that the measurement parameters a_2 and a_3 would reduce the absorbed power generally. At the same time, the obtained sub-optimal solution base on LQG, full state observation is compared to the optimal solution obtained by nonlinear programming. The details of the nonlinear programming algorithm has been given in an appendix.

In order to investigate the broad-banded wave, the wave condition with $H_s = 3\text{m}, T_p = 7.42\text{s}$ and $\gamma = 1$ has also been considered. Fig. 12 shows the trajectories of $v(t)$ and $\dot{v}(t)$, control force $f_c(t)$ and instantaneous absorbed power $P(t)$ at optimal control. The mean absorbed power is also shown in Table 2. As seen, The same analysis results are applied to the extreme broad-banded wave.

Given a sea-state defined by the parameters H_s, T_p, and γ a sufficient long realization of $f_e(t)$ is generated from Eqs. (26) and (29) using a so-called broken line equivalent white noise process for $w_1(t)$ (Nielsen and Zhang, 2017). Next, the load realization applied in LQG control is used for the nonlinear programming solution for the optimal solution. Finally, q and r are determined so the
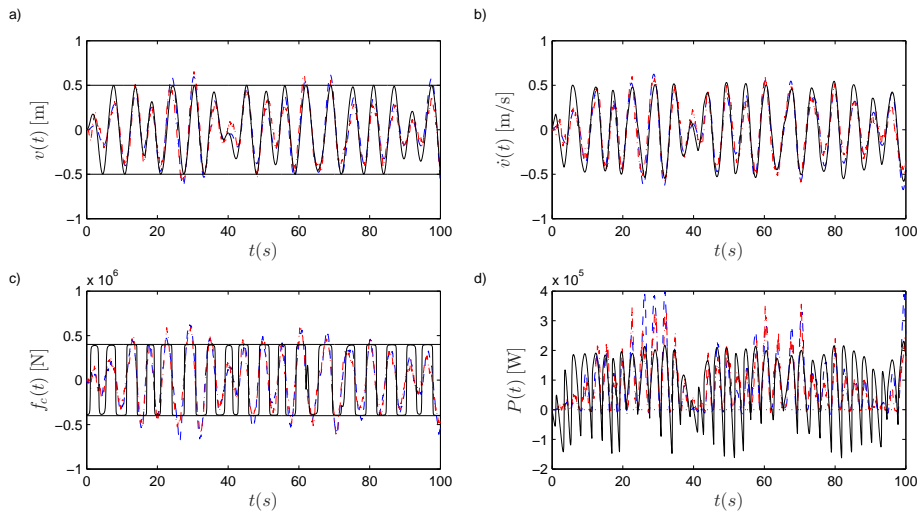
Figure 12: The trajectories of $v(t)$ and $\dot{v}(t)$, control force $f_c(t)$ and instantaneous absorbed power $P(t)$ at optimal control. $H_s = 3$m, $T_p = 7.42$s and $\gamma = 1$. $f_{c,\max} = -f_{c,\min} = 4 \times 10^5$N and $v_{\max} = -v_{\min} = 0.5$m. a) $v(t)$. b) $\dot{v}(t)$. c) $f_c(t)$. d) $P(t)$. ——: Nonlinear programming solution. - - - : LQG, full state observation. -·-·-·: LQG, partial state observation.

standard deviations σ_v and σ_{f_e} are identical for the nonlinear programming solution and the LQG solution with full state observation. When nonlinear programming is applied, the computational cost grows exponentially with the length of the control horizon. For this reason stable solutions for the parameters q and r can't be achieved by merely using a single realization of the wave stationary load process $f_e(t)$ of limited length. Instead a finite number N of independent time series of the wave load of limited length should be generated, which from samples of q and r are generated based on nonlinear programming. Next, stable estimates of q and r may be obtained as ensemble averages of the indicated sample values. Then, the calculation time of the approach merely growth linearly with N. Assuming that all involved stochastic processes are ergodic it doesn't matter which realization of $w_1(t)$ (and hence of $f_e(t)$) is used. The indicated standard deviations are determined by time-averages of $N = 6$ independent time series of $v(t)$ and $f_c(t)$ in the interval [0, 100s] where the time step $\Delta\tau$ is $\frac{T_p}{150}$. Further, according to the Pontryagin's maximum principle (Pontryagin et al., 1962), the optimal control is obtained for the maximum value of the Hamiltonian as given by Eq. (35). Then, an increase or decrease of the weights q and r implies a decrease or increase of $v(t)$ and $f_c(t)$ at optimal control. In the present model it follows that q and r are negative correlated to the magnitude of the constraints on the displacement and control force.

In Fig. 11d, at optimal control $P(t)$ may have negative loops. Actually, an imposed constrain $f_c(t) \equiv 0$, corresponding to $P(t) \equiv 0$ during a time interval with negative power absorption in the optimal control, will produce a non-optimal velocity trajectory $\dot{v}(t)$ out-side the said time interval via the impact on the equation motion Eq. (12), resulting in a reduced average absorbed power during a longer control horizon. The same observation was made by Falnes (Falnes, 2002).

25

7. Conclusions

In this paper, a control law based on the LQG approach is used to maximize the absorbed energy of a wave energy point absorber system. As a result of rational approximations to the radiation force and the wave load, the integrated dynamic system is reformulated as a linear stochastic differential equation which is driven by a unit intensity Gaussian white noise. Further, the Kalman filter technique is employed to estimate the combined state vector based on noise observation of $v(t)$ and $\dot{v}(t)$. The proposed LQG control successfully demonstrated the ability to extract and maximize the absorbed power while keeping the absorber motion and control force small. Based on a specific calibration technique of the parameters q and r entering the performance functional of the LQG solution close to optimal control force solutions are generated in cased of low signal to noise ratios of the observed state variables. For higher noise level a certain reduction appears in the absorbed power.

Appendix: Nonlinear programming algorithm

The optimal control problem in Eq. (12) is reformulated as a nonlinear programming problem by discretizing the objective functional and the state

vector in time:

$$\max \quad J\big(\mathbf{X}(\tau_M)\big) \; = \; x_{n+3}(\tau_M)$$

subject to the path and inequality constraints :

$$\left. \begin{aligned} \mathbf{c}\big(\mathbf{X}(\tau_j)\big) \; &= \; \mathbf{0} \\[6pt] \mathbf{h}\big(\mathbf{X}(\tau_j)\big) \; &= \; \begin{bmatrix} v(\tau_j) \; - v_{\max} \\ - v(\tau_j) \; + v_{\min} \\ f_c(\tau_j) - f_{c,\max} \\ - f_c(\tau_j) + f_{c,\min} \end{bmatrix} - \mathbf{s}(\tau_j) = \mathbf{0} \\[6pt] \mathbf{s}(\tau_j) \qquad &\geq \; \mathbf{0} \end{aligned} \right\} \tag{55}$$

where $\tau_j \; = \; t_0 \; + \; j \, \Delta\tau \; , \; j \; = \; 0, 1, \ldots, M.$

$\mathbf{s}(t)$ indicates a vector function of slack variables. The time step in the discretization of the interval $]t_0, t_1]$ is given as $\Delta\tau = \frac{t_1 - t_0}{M}$. The vector $\mathbf{X}(t)$ of dimension $2n + 6$ and the path constrain vector $\mathbf{c}\big(\mathbf{X}(t)\big)$ of dimension $n + 3$ are defined as:

$$\mathbf{X}(t) \; = \; \left[v(t) \, , \, \dot{v}(t) \, , \, \mathbf{z}_r^T(t) \, , \, x_{n+3}(t) \, , \, \frac{d}{dt}v(t) \, , \, \frac{d}{dt}\dot{v}(t) \, , \, \frac{d}{dt}\mathbf{z}_r^T(t) \, , \, \frac{d}{dt}x_{n+3}(t) \right]^T \tag{56}$$

$$\mathbf{c}\big(\mathbf{X}(t)\big) \; = \; \begin{bmatrix} \frac{d}{dt}v(t) \; - \; \dot{v}(t) \\[4pt] M\frac{d}{dt}\dot{v}(t) \; + \; \mathbf{p}_r \, \mathbf{z}_r(t) \; + \; r\big(v(t)\big) \; - \; f_e(t) \; + \; f_c(t) \\[4pt] \frac{d}{dt}\mathbf{z}_r(t) \; - \; \mathbf{A}_r \, \mathbf{z}_r(t) \; - \; \mathbf{b}_r \, \dot{v}(t) \\[4pt] \frac{d}{dt}x_{n+3}(t) \; - \; f_c(t) \, \dot{v}(t) \end{bmatrix} \tag{57}$$

The inherent approximation in the indicated nonlinear programming formulation concerns the discretization of the time continuous problem into $M + 1$ discrete instants of time for optimization, and the use of the rational approximation in Eq. (18) for the force $f_{r,0}(t)$.

The formulation applies to both displacement constraints and control force constraints. In case, merely control force constraints are prescribed the algo-

rithm is applied by using large values of $v_{\max}$ and small values of $v_{\min}$.

The applied algorithm for solving the indicated nonlinear programming problem is described in (El-Bakry et al., 1996).

References

Archimedes Wave Swing, 2004. Archimedes Wave Swing <http://www.awsocean.com/>.

Basu, B., Staino, A., 2016. Control of a Linear TimeVarying System With a Forward Riccati Formulation in Wavelet Domain. Journal of Dynamic Systems, Measurement, and Control, ASME, 138 (10), 104502.

Cummins, W., 1962. The impulse response functions and ship motions. Schiffstechnik 9, 101109.

Cretel, J.A., Lightbody, G., Thomas, G.P., Lewis, A.W., 2011. Maximisation of energy capture by a wave-energy point absorber using model predictive control. IFAC Proceedings Volumes, 44(1), 3714-3721.

El-Bakry, A. S., Tapia, R. A., Tsuchiya, T., Zhang, Y., 1996. On the formulation and theory of the Newton interior-point method for nonlinear programming. Journal of Optimization Theory and Applications, 89(3), 507-541.

Falnes, J., 2002. Ocean Waves and Oscillating Systems: Linear Interactions Including Wave-Energy Extraction. Cambridge University Press.

Faltinsen, O., 1990. Sea Loads on Ships and Offshore Structures. Cambridge University Press.

Hals, J., Falnes, J., Moan, T., 2011. Constrained optimal control of a heaving buoy wave-energy converter. Journal of Offshore Mechanics and Arctic Engineering, 133(1), 011401.

Hartl, R.F., Sethi, S.P., Vickson,R.G., 1995. A survey of the maximum principles for optimal control problems with state constraints. SIAM review, 37(2), 181-218.

Lattanzio, S.M., Scruggs, J.T., 2011. Maximum power generation of a wave energy converter in a stochastic environment. In Control Applications (CCA), 2011 IEEE International Conference on (pp. 1125-1130). IEEE.

Scruggs, J.T., Lattanzio, S.M., Taflanidis, A.A., Cassidy, I.L., 2013. Optimal causal control of a wave energy converter in a random sea. Applied Ocean Research, 42, 1-15.

Kassem, A.M., Besheer, A.H., Abdelaziz, A.Y., 2015. A linear quadratic gaussian approach for power transfer maximization of a point absorber wave energy converter. Electric Power Components and Systems, 43(8-10), 1173-1181.

Hasselmann K., Barnett, T.P., Bouws, E., et al., 1973. Measurements of wind wave growth and swell decay during the Joint North Sea Project (JONSWAP). Deutches Hydrographisches Institut.

Li, G., Weiss, G., Mueller, M., Townley, S., Belmont, M.R., 2012. Wave energy converter control by wave prediction and dynamic programming. Renewable Energy, 48, 392-403.

Mathworks, 2011. Control System Toolbox 9.1. Mathworks, Inc.

Meirovitch, L., 1990. Dynamics and Control of Structures. John Wiley & Sons.

Newman, J., 1977. Marine Hydrodynamics. The MIT Press.

Nielsen, S.R.K., Zhang, Z., 2017. Stochastic Dynamics. Aarhus Unversity Press.

Nielsen, S.R.K., Zhou, Q., Kramer, M.M., Basu, B., Zhang, Z., 2013. Optimal control of nonlinear wave energy point converters. Ocean Engineering 72, 176-187.

Ozkop, E., Altas, I.H., 2017. Control, power and electrical components in wave energy conversion systems: A review of the technologies. Renewable and Sustainable Energy Reviews, 67, 106-115.

Pelamis Wave, 2012. Pelamis Wave Power <http://www.pelamiswave.com/>.

Pontryagin,L.S., Boltyanskii,V.G., Gamkrelitze,R.V., Mishenko,E.F., 1962. The Mathematical Theory of Optimal Processes, Interscience Publishers, John Wiley and Sons, New York.

Ringwood, J.V., Bacelli, G., Fusco, F., 2014. Energy-maximizing control of wave-energy converters: The development of control system technology to optimize their operation. IEEE Control Systems, 34(5), 30-55.

Sichani, M.T., Chen, J.B., Kramer, M.M., Nielsen, S.R.K., 2014. Constrained optimal stochastic control of non-linear wave energy point absorbers. Applied Ocean Research, 47, 255-269.

WAMIT, 2011. WAMIT User Manual, version 7.0. Technical Report.

Wang, L., Engström, J., Göteman, M., Isberg, J., 2015. Constrained optimal control of a point absorber wave energy converter with linear generator. Journal of Renewable and Sustainable Energy, 7(4), 043127.

Wavedragon, 2005. Wave Dragon <http://www.wavedragon.net/>.

Wave Star Energy, 2003. Wave Star Energy <http://wavestarenergy.com/>.

Zou, S., Abdelkhalik, O., Robinett, R., Bacelli, G., Wilson, D., 2017. Optimal control of wave energy converters. Renewable Energy, 103: 217-225.